

## Article

# Research on Optical Diagnostic Method of PDE Working Status Based on Visible and Near-Infrared Radiation Characteristics

Xiaolong Huang, Ning Li \* and Yang Kang

National Key Laboratory of Transient Physics, Nanjing University of Science and Technology, Nanjing 210094, China; huang\_xl@njjust.edu.cn (X.H.); vince\_kang@126.com (Y.K.)

\* Correspondence: lining@njjust.edu.cn

**Abstract:** Fill fraction not only has a profound impact on the process of deflagration to detonation in pulsed detonation engine, but also affects the propulsion performance in both flight and ground tests. In this paper, a novel optical diagnostic method based on detonation exhaust radiation in visible and near-infrared region within 300–2600 nm is developed to determine the current working state in the gas–liquid two-phase pulsed detonation cycle. The results show that the radiation characteristic in each stage of detonation cycle is unique and can be a good indicator to infer the fill fraction. This is verified experimentally by comparison with the laser absorption spectroscopy method, which utilizes a DFB laser driven by ramp injection current to scan H<sub>2</sub>O transition of 1391.67 nm at a frequency of 20 kHz. Due to concentrated radiation intensity, time duration reaching accumulated radiant energy ratio of 50% in detonation status would be smaller than 1.2 ms, and detonation status would be easily distinguished from deflagration with this critical condition. In addition, the variation of important intermediates OH, CH, and C<sub>2</sub> radicals during detonation combustion are obtained according to the analysis of detonation spectrum, which can also be proposed as a helpful optical diagnostics method for the combustion condition based on C radical concentration. The study demonstrates the feasibility of optical diagnostics based on radiation in visible and near-infrared regions, which could provide an alternative means to diagnose and improve pulsed detonation engine performance.

**Keywords:** pulse detonation engine (PDE); near-infrared; visible light; fill fraction; optical diagnostics



**Citation:** Huang, X.; Li, N.; Kang, Y. Research on Optical Diagnostic Method of PDE Working Status Based on Visible and Near-Infrared Radiation Characteristics. *Energies* **2021**, *14*, 5703. <https://doi.org/10.3390/en14185703>

Academic Editor: Giuseppe Pascazio

Received: 9 August 2021

Accepted: 7 September 2021

Published: 10 September 2021

**Publisher's Note:** MDPI stays neutral with regard to jurisdictional claims in published maps and institutional affiliations.



**Copyright:** © 2021 by the authors. Licensee MDPI, Basel, Switzerland. This article is an open access article distributed under the terms and conditions of the Creative Commons Attribution (CC BY) license (<https://creativecommons.org/licenses/by/4.0/>).

## 1. Introduction

A detonation wave is a kind of supersonic combustion wave that consists of shock waves driven by energy release from closely coupled chemical reactions, which has broad application prospects in the field of aerospace propulsion technology [1–5]. As one of the innovative propulsion devices, a pulse detonation engine (PDE) generates thrust by using detonation waves and has attracted great attention due to its simple structure and high thermodynamic cycle efficiency [6–8].

Fill fraction is one of the critical factors among all kinds of factors affecting PDE propulsion performance. Kim [9] carried out a series of experiments with operating frequencies of 40, 80, 120, 160, and 200 Hz. Results showed that a low fill fraction resulted in an incidence ratio (less than 50%) at the operating frequency of 200 Hz. Anand [10] investigated a circular array of six pulse detonation combustors that integrated to an axial turbine to extract power from the detonative combustion process. It was experimentally proven that fill fraction would affect the exploration of the axial turbine. Furthermore, Anand [11] investigated the effect of multiple facets of pulse detonation combustors on its acoustic signature and pointed out that shock strength is weakened by decreasing the fill fraction due to shock decay, which occurs over the unfilled portion of the detonation tube.

Moreover, the deflagration to detonation transition would be impossible if the fill fraction was extremely low. Haghdoost [12] conducted an experiment on flow dynamics during one full pulsed detonation cycle via high-speed particle image velocimetry, and the deflagration was observed when fill fraction could not satisfy the distance of deflagration

to detonation transition requirement. Bradley [13] verified the deflagration to detonation transition was possible if autoignition of the reactants occurred in the time available and if the projected flame speed approached the Chapman–Jouguet velocity at the same temperature and pressure.

Traditional contact measurement methods, such as piezoelectric transducers and ion probes, can only obtain a change of pressure or ion in the detonation cycle. It is extremely difficult to measure and control the fill fraction with high precision due to unfavorable measurement conditions in harsh environments, such as strong vibration, high temperature when detonation exhaust rushes out, and transient variation in pressure. Recently, laser absorption spectroscopy has been generally developed as a useful tool to record the gas concentration and temperature due to its advantages of extremely fast response speed and extremely high environmental adaptability [14–20]. Hinckley et al. [21] used a DFB laser to measure the temperature in the detonation tube, which provided more direct measurement data to monitor the state of PDE combustion. Ma et al. [22] used a 1.6  $\mu\text{m}$  semiconductor laser to analyze the filling process of fuel ( $\text{C}_2\text{H}_4$ ) in the working process of the pulse detonation engine and obtained the change of equivalent ratio when valve was opened and closed. By controlling the working time of fuel valve and ignition, the fuel waste was minimized. Li et al. [23,24] used water molecular absorption lines of  $7185.6\text{ cm}^{-1}$  and  $7444.35\text{ cm}^{-1}$  to carry out the online monitoring of  $\text{H}_2\text{O}$  concentration changes in the valve-less gas–liquid two-phase PDE and proposed a test method of fill fraction based on tunable diode laser absorption spectroscopy to analyze the influence of fill fraction on PDE impulse.

However, there are still some stringent requirements when the laser absorption method applies. For instance, reliable observation windows must be designed on the detonation tube for laser beam transmission, which should be able to withstand the severe test of high temperature and pressure in detonation exhaust. In addition, there is another challenge to reduce the contamination of windows from soot generated from liquid fuel detonation. It is difficult to popularize this technique in field tests of the detonation engine.

In fact, an optical diagnostic method based on radiation analysis of combustion exhaust has been proven to be an effective way to provide transient flow information in the detonation cycle. Rankin et al. [25,26] used the mid-infrared imaging to investigate the structure of detonation waves propagating through the annular channel of a rotating detonation engine. They found that the photodiode signals were different at various angles, and with periodical appearance of the detonation wave fronts, the time-dependent photodiode signals increased rapidly, then the signals decayed exponentially. The results showed that the mid-infrared images provided useful insights for improving fundamental understanding of the detonation structure in detonation flow.

In this paper, a novel optical diagnostic method based on detonation exhaust radiation in visible and near-infrared region is developed to determine the current working state in the gas–liquid two-phase pulsed detonation cycle. The unique radiation characteristic in each stage of the detonation cycle would be a good indicator to infer the current fill fraction. Detonation status would be easy to distinguish from deflagration based on the analysis of the accumulated radiant energy after the detonation wave arrives. Furthermore, the chemical reaction mechanism in detonation combustion would be investigated by analysis of radicals and other intermediate products using high resolution spectrometer. The research could provide reliable data support for the improvement of PDE work efficiency and optimization of operation control.

## 2. Methodology

### 2.1. PDE Test System and Experimental Setup

The schematic diagram of the gas–liquid two-phase PDE detonation gas test system is shown in Figure 1, which consists of the detonation tube, the photoelectric detector, the optical adjustment frame, the detonation pressure test system, the high-resolution spectrometer, and the data acquisition system.

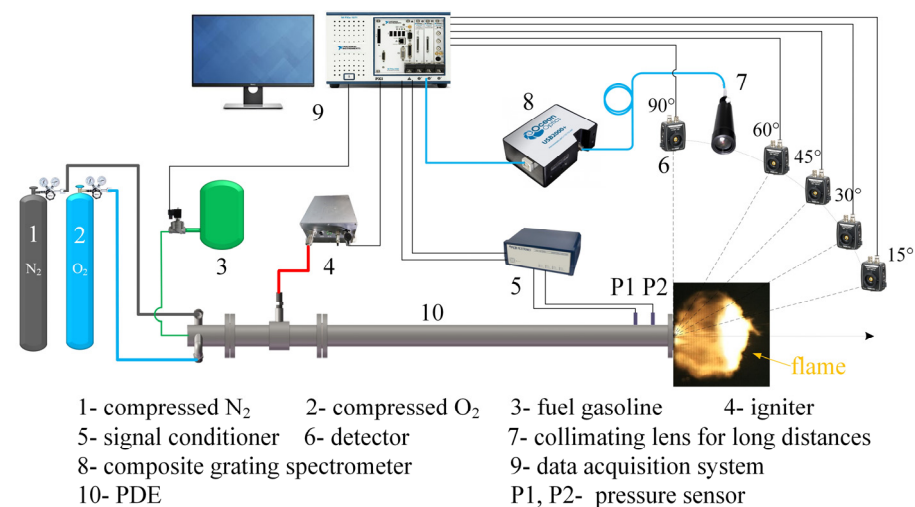


**Figure 1.** The schematic diagram of the experiment setup.

During the experiment, liquid gasoline was chosen as the fuel, and the oxidant was the mixture of nitrogen and oxygen (oxygen content is about 25%). Both fuel and oxidant were injected into the fill section on the left side of PDE. The mixture of the fuel and oxidant was achieved by combining the atomizing nozzle and venturi tube in the mixing section. Once the mixture was ignited in the ignition section, the deflagration was transformed to detonation under the action of the orifice plate obstacle configuration with 0.43 blockage ratio. Then, the detonation wave propagated downstream until outside the tube, and the pressure, as well as the temperature in the tube, decayed to the ambient conditions.

The detonation tube was placed horizontally, where the diameter and length of the tube were 80 mm and 1500 mm, respectively. The pressure of detonation was determined by two PCB 113B24 pressure sensors with a maximum measurement pressure of 1000 psi (6895 kPa). The sensor P2 was arranged near the exit of the tube, and the distance between P1 and P2 was 100 mm. The visible light radiation test adopted the PDA36A Si photodetector of Thorlabs company, and the wavelength response range was 350–1100 nm. The PDA50B Ge photodetector and PDA10D InGaAs photodetector of Thorlabs company were used in the near infrared radiation test, whose wavelength response ranges were 800–1800 nm and 1.2–2.6  $\mu\text{m}$ , respectively. The photodetectors were horizontally arranged in the directions of 15°, 30°, 45°, 60° and 90°, whereas the photodetectors were 3 m away from the tube exit and had the same height as the PDE.

The spectrometer was selected as the HR2000+ composite grating spectrometer of Ocean Optics company, whose spectral range is 200–1100 nm, resolution is 0.5 nm, and core diameter of transmission fiber is 400  $\mu\text{m}$ . During the experiment, the detonation flame spectrum signal was collected and input to the optical fiber through the collimating lens, where the collimating lens and the detectors were arranged symmetrically to the tube exit. Due to the lack of gated detection technology, the integration time of the spectrometer was set to 5 ms. The data from PCB pressure, photodetector, and spectrometer were acquired simultaneously on eight channels of a National Instruments PXIe-1062Q acquisition system with a 500 k sampling rate.

## 2.2. PDE Cycle and Fill Fraction Measurement System

The valveless PDE cycle is divided into four processes, as depicted in Figure 2a. Process I: The combustible mixture of fuel and oxidant were filled into the PDE detonation tube from the left of the tube until the tube was filled with mixture. Process II: Once the combustible mixture was ignited in the ignition section, the deflagration was transformed to detonation under the action of the orifice plate obstacle configuration. Then, the detonation wave propagated downstream to the tube exit. Process III: The detonation wave exited from the tube, and the expansion wave propagated upstream to the left of the tube.

Process IV: The detonation products were exhausted from the tube, and the fill process of the next cycle started.

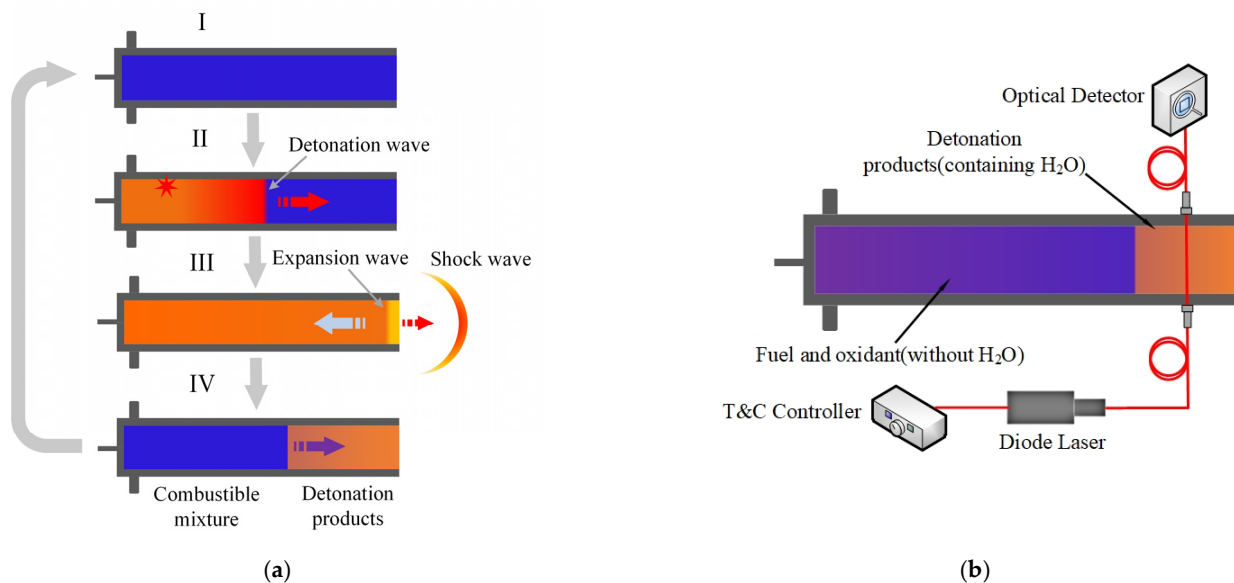


**Figure 2.** (a) Schematic of the valveless PDE cycle, (b) the schematic diagram of fill fraction measurement system based on laser absorption spectroscopy.

The fill fraction ( $ff$ ) of fuel and oxidant mixture has an important influence on the intensity of detonation wave formed in detonation tube. As the content of H<sub>2</sub>O in the detonation product is obviously higher than that in the mixture of fresh fuel and oxidant, the content of H<sub>2</sub>O can be used as the object to determine the fill process. In order to study the radiation characteristics of gas–liquid two-phase PDE under different fill fractions, the fill fraction measurement system of PDE was built based on a single optical path fiber distributed laser absorption spectroscopy [27], as shown in Figure 2b. The laser with center wavelengths of 1391.67 nm was selected to measure the absorption peak of H<sub>2</sub>O. The H<sub>2</sub>O absorption transition was scanned with high frequency by a narrow-linewidth laser, which was driven by ramp injection current. The absorption signal with Voigt lineshape appeared in the time–domain curve. The signal intensity depended on spectroscopic data (linestrength, lower energy state, linewidth, etc.) and environment parameters (concentration, temperature, pressure, path length). The H<sub>2</sub>O concentration was inferred according to this absorbance recovered by polynomial fitting of the non-absorption region of the curve. Then, the absorption of H<sub>2</sub>O was a good indicator to estimate the existence of detonation exhaust, which in turn decided the current state in the whole detonation cycle. Figure 3 plots the laser signal of high frequency wavelength scanning with H<sub>2</sub>O absorption peak and without H<sub>2</sub>O absorption peak during detonation. Once the filling process of the mixture of fresh fuel and oxidant was measured, the fill fraction could be calculated.

### 2.3. Approach and Equation

#### 2.3.1. The Normalization of Radiation Intensity

In order to explore the radiation characteristics of gas–liquid two-phase detonation at different directions, the radiation signals of the detonation process were measured in directions of 15°, 30°, 45°, 60° and 90°, respectively.

The normalization of radiation intensity at the different direction angles was carried out based on the radiation intensity  $I^{15^\circ}$  to analyze the variation law of directivity, where  $I^{15^\circ}$  is the radiation intensity in direction 15°. The normalization expression is:

$$\bar{I}^\theta = I^\theta / I^{15^\circ} \quad (1)$$

where  $I^\theta$  is the radiation intensity in direction  $\theta$ ,  $\bar{I}^\theta$  is the normalized dimensionless radiation intensity.

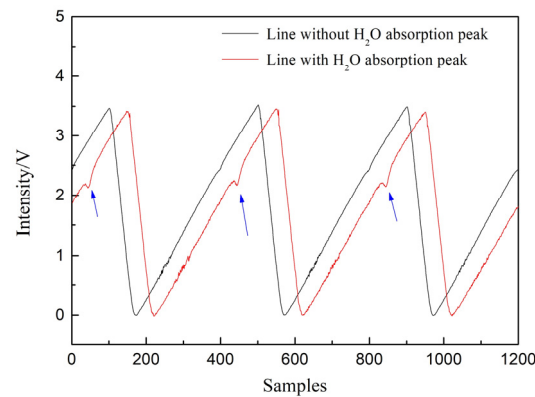


**Figure 3.** Laser signal of high frequency wavelength scanning.

### 2.3.2. Definition of Radiant Energy

In order to identify the combustion mode based on the radiation signals of detonation and deflagration, the radiation signals within 5 ms after the wave overflowed the tube exit were selected for analysis. The radiant energy  $E_t$  at time  $t$  was obtained by integrating the radiation intensity  $I$ , i.e.:

$$E_t = \int_0^t I dt \quad (2)$$

The ratio  $\eta$  is defined as

$$\eta = \frac{E_t}{E_0} = \frac{\int_0^t I dt}{\int_0^{5\text{ms}} I dt} \quad (3)$$

where  $E_0$  is the radiant energy at 5 ms, and  $E_0$  is variable for different fill fractions.

## 3. Results and Discussion

### 3.1. Radiation Signals

Figure 4 plots the pressure signal measured by sensor P2 in the detonation tube exit and the radiation signal measured by three wave band detectors in  $90^\circ$  direction of a single cycle detonation. The plot shows that the pressure signal and the radiation signal are synchronous, i.e., the pressure signal rises rapidly, and the radiation signal rises synchronously when the detonation wave arrives. The rising edge time and the duration time in the pressure curve were about  $8 \mu\text{s}$  and  $3.8 \text{ ms}$ , respectively. The rising edge time of radiation signals was about  $30\text{--}50 \mu\text{s}$ , and the corresponding duration time was  $3\text{--}3.8 \text{ ms}$ . When the detonation waves exited the detonation tube, the high-temperature and high-pressure gas was exhausted out of the tube, and the radiation signal increased slightly under the action of the high-temperature and high-pressure gas. Then, the pressure in the tube gradually decreased to the ambient pressure, the filling process of fresh fuel oxidant and the exhausting process of detonation products began while the residual high temperature detonation products in the tube were gradually exhausted out of the tube. Due to the strong radiation of the high temperature detonation products, the radiation signal rose again. After  $183 \text{ ms}$  of detonation wave exiting from the tube, the detonation products were completely exhausted from the detonation tube, and the radiation signal intensity decreased to the initial value.

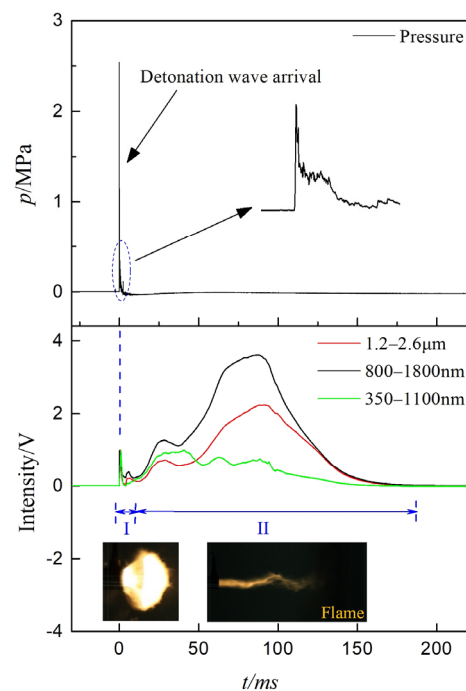


**Figure 4.** Curves of detonation pressure and radiation signal at different processes. (I: detonation wave exits from the tube; II: detonation products exhaust from tube).

As shown in Figure 4, the radiation signals in different spectral bands have obvious differences in the exhaust process of high temperature detonation products. In the 350–1100 nm band, the radiation signal of high temperature detonation products reached the peak value at 40 ms of the exhaust process, and the corresponding radiation intensity was comparative with the radiation intensity of detonation waves. In the 800–1800 nm and 1.2–2.6 μm near infrared bands, the radiation signal of high temperature detonation products reached the peak value after 86 ms and 91 ms of the exhaust process, respectively, and the corresponding radiation intensities were 3.6 and 2.2 times the radiation signals of detonation waves.

The reason for the differences is that the intensity of the visible radiation signal is mainly determined by the temperature of high-temperature detonation products, while the intensity of infrared radiation signal is not only determined by the temperature. In the exhaust process of high-temperature detonation products, the temperature of high-temperature detonation products decreased continuously, and the intensity of the visible radiation signal decreased with the decrease of the temperature. However, there were large numbers of carbon particles in the detonation products fueled by gasoline, where the radiation signal of carbon particles in the infrared band was much larger than that in the visible band. Therefore, although the temperature decreased in the later process of the exhaust process, the radiation signal in infrared band increased to the peak value again due to the obvious emission of carbon particles, which resulted in the radiation signal intensity being significantly greater than at the arrival time of the detonation wave. The corresponding time of peak radiation signal in infrared band was delayed compared with that in visible band.

### 3.2. Distribution Characteristics of Radiation Space

According to the the normalization of radiation intensity equation in Equation (1), the directivity distribution of radiation signals in different bands are calculated and shown in Figure 5a. It shows that with the increase of the direction angle, the radiation signal intensities caused by the process of detonation waves exiting and detonation products exhausting in the three bands decrease gradually. Compared with the radiation intensity produced by the detonation wave, the radiation intensity decay rate produced by deto-

nation products is faster. Taking the 1.2–2.6  $\mu\text{m}$  band as an example, the radiation signal intensity of detonation waves and detonation products in the  $90^\circ$  direction was attenuated by 45% and 62%, respectively, compared with those in the  $15^\circ$  direction.

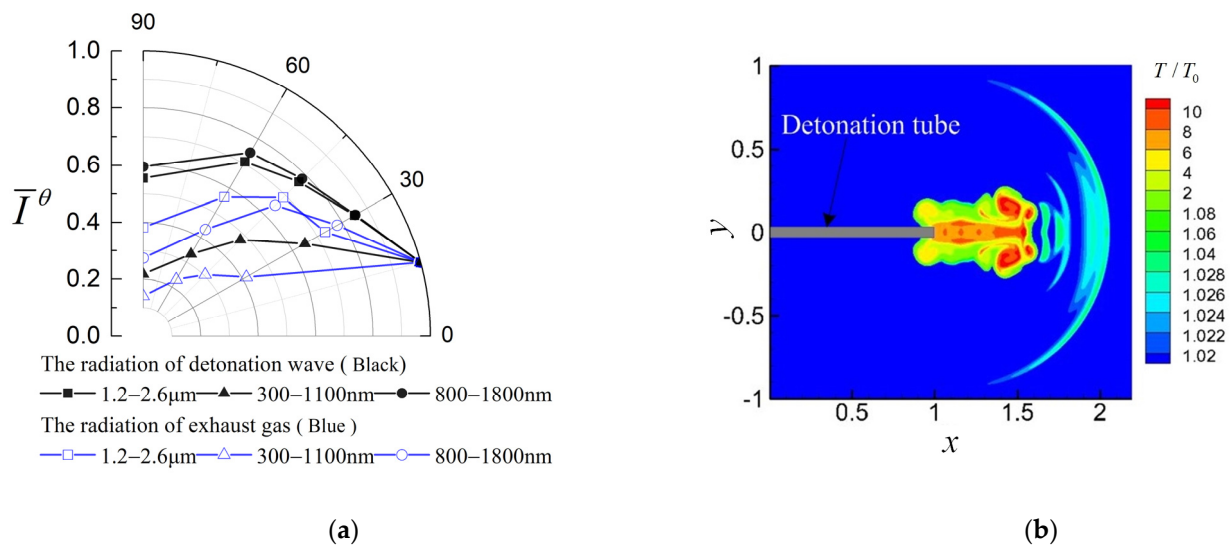


**Figure 5.** (a) Directivity distribution of radiation signals in different bands, (b) Temperature nephogram of detonation.

In order to study the variation of the flow field outside the detonation tube and the directivity of detonation radiation with the variation of propagation distance, the outflow field of PDE has been simulated by a space–time conservation element and solution element method numerically. Figure 5b is the simulated temperature distribution of the outflow field when the detonation waves overflow outside the tube. The plot shows that the temperature distribution on the surface of the shock wave formed by the degenerated detonation wave is uniform; therefore, the difference of the radiation signal intensity caused by detonation waves is relatively small at different direction angles. However, the high temperature detonation products are concentrated in the direction of the central axis, and the high temperature region is also distributed in the central region of the jet near the tube axis. Therefore, the radiation intensity produced by high-temperature detonation products in the  $15^\circ$  direction is greater than that in the  $90^\circ$  direction. This is the main reason for the obvious differences of the radiation signals of detonation products at different directions.

#### 4. Optical Diagnostic Method Based on Radiation

##### 4.1. Fill Fractions

In this section, the fill fraction in the multi-cycle working process of detonation engine is measured by laser absorption spectroscopy, and the relationship between radiation time domain signal and fill fraction is analyzed. Since PDA36A Si photodetector has a fast response velocity to hydrocarbon fuel combustion products, the 350–1100 nm band radiation intensity signal in the  $90^\circ$  direction was selected for analysis.

Figure 6a plots the pressure signal and 350–1100 nm band radiation signal collected by sensor P2 and Si photodetector, respectively. With the periodic operation of PDE, the pressure signal and radiation signal of sensor P2 showed periodic variations. When the detonation wave propagated to the tube exit, the pressure at the pressure sensor P2 rose rapidly, and the radiation signal in the 350–1100 nm band also rose rapidly. The detonation waves degenerated into shock waves without chemical reaction due to the loss of fuel support when the detonation waves exited from the detonation tube. The pressure and temperature of detonation waves dropped rapidly, and the radiation signal also dropped rapidly. The duration of the rising edge in the sensor P2 pressure curve was about 8  $\mu\text{s}$ , and the duration of the pressure drops to the minimum value was about 3.8 ms. The radiation signal curve rose rapidly, where the duration of the rising edge was about 0.98 ms and the

duration of radiation intensity drops to the minimum value was 5.71 ms. The duration of the radiation signal was prolonged compared with that of the pressure signal as the radiation signal was caused by the detonation wave and the followed detonation products.

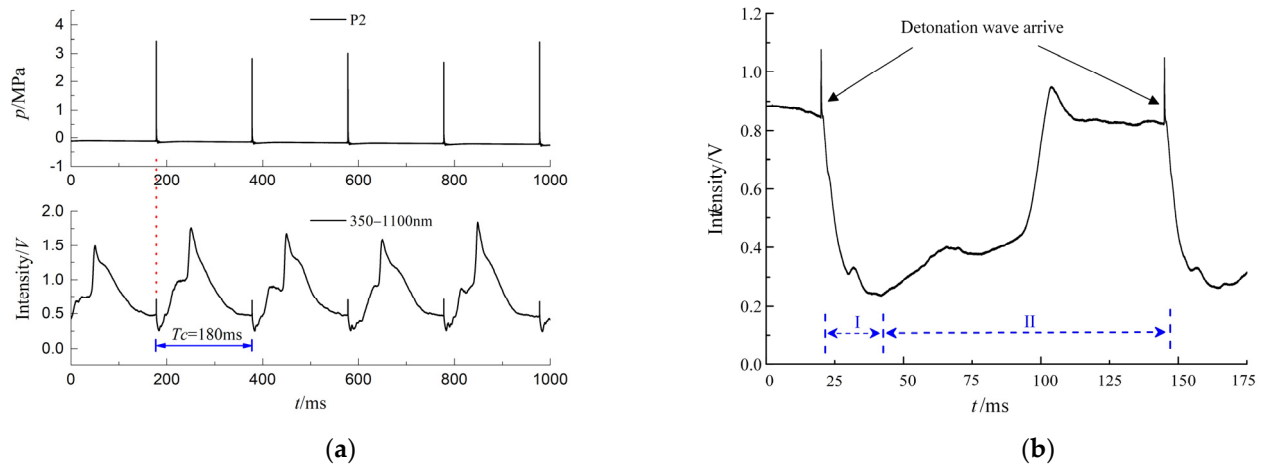


**Figure 6.** (a) Radiation signal under multi-cycle detonation, (b) Radiation signal with fill fraction 70%. (I: detonation wave exits from the tube; II: detonation products exhaust from tube).

With the ending of the outward expansion process of high-temperature and high-pressure gas, the pressure in the detonation tube decreased to the ambient pressure. However, there were still large amounts of higher temperature atmospheric gas in the tube. As the residual high-temperature gas was gradually exhausted outward, the radiation generated by various combustion products made the radiation signal rise again. After 45 ms of the detonation wave exiting from the tube, the radiation signal rose to the maximum value and then decreased gradually. After 180 ms of the detonation wave exiting from the tube, the detonation combustion products were completely exhausted from the tube and the radiation intensity decreased to the ambient value. Then, the PDE began the next working cycle.

The single working cycle period  $T$  of detonation tube was obtained as 183 ms by analyzing the time domain signal of a single cycle detonation radiation signal in Figure 4, and the ignition time interval  $T_c$  was obtained as 180 ms from the multi-cycle detonation radiation signal in Figure 6a. Then, the fill fraction  $ff$  of the detonation tube could be accurately calculated as 98.36% by using  $ff = T_c/T$ . Therefore, the measurement error for multi-cycle condition by using the method of detonation radiation signal and laser absorption spectroscopy is about 1.64%, as the fill fraction measured by laser absorption spectroscopy is about 100%.

Figure 6b shows the radiation signal in the 350–1100 nm band for fill fraction 70% measured by laser absorption spectroscopy, which is obviously different from that shown in Figure 6a. For a fill fraction of 100%, as shown in Figure 6a, the high-temperature gas was completely exhausted after 183 ms, and the radiation signal decreased to the initial value. However, for a fill fraction of 70%, as shown in Figure 6b, the detonation wave of the next working cycle reached the tube exit when the high-temperature gas was exhausted only for 128 ms, i.e.,  $T_c = 128$  ms. Then, the fill fraction  $ff$  of detonation tube could be accurately calculated as 69.95% by using the method of detonation radiation signal. Therefore, the fill fraction can be measured by the method of detonation radiation signal.

#### 4.2. Detonation and Deflagration

For small fill fraction or large atomized particles of liquid fuel, the detonation waves cannot be formed in the detonation tube, and the combustion mode is deflagration with low thermal cycle efficiency. Compared with detonation waves, the deflagration wave has lower pressure and slower propagation velocity. The traditional method to identify the detonation state is to use the adjacent pressure sensors (P1, P2) to obtain the pressure

and wave velocity in the tube first, then compare the pressure and the wave velocity with the C-J detonation pressure and wave velocity to judge whether the combustion mode in the detonation tube has reached the detonation state. As shown in Figure 7, the pressure peak can be obtained directly.  $\Delta t$  is the time interval of the combustion wave arrivals to P1 and P2.  $\Delta d$  is the distance between P1 and P2. The velocity of the combustion wave  $v$  is calculated as  $v = \Delta d / \Delta t$ .

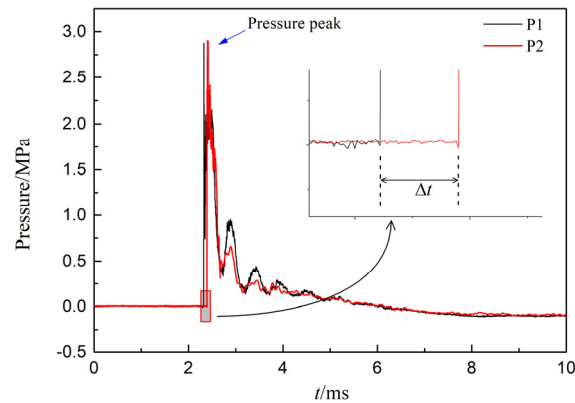


Figure 7. The pressure curves of P1 and P2.

However, the traditional method is a conventional contact test method and is sensitive to the ambient temperature. In this section, the spectral radiation method based on the radiation signal in 350–1100 nm band is presented to identify the combustion mode.

Figure 8 shows the radiation signal in 350–1100 nm band of deflagration and detonation. The plots show that for detonation waves overflowing the tube exit, the radiation signal rose rapidly, and the rising edge time was about 45  $\mu$ s, while for deflagration waves overflowing the tube exit, the radiation signal rose slowly, and the rising edge time was 2.6 ms. The results also show that the radiation signal intensity produced by detonation waves was much higher than that of deflagration waves. It is mainly because that detonation is similar to constant volume combustion, where the temperature and pressure are much higher than that of deflagration. Therefore, the radiation signal intensity of detonation is higher than that of deflagration. Figure 8 also shows that the radiation duration generated by detonation wave and deflagration wave was basically maintained at 4–6 ms when the waves overflowed from the tube exit.

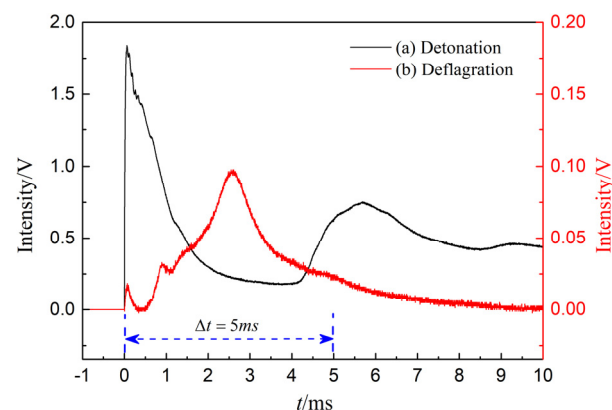
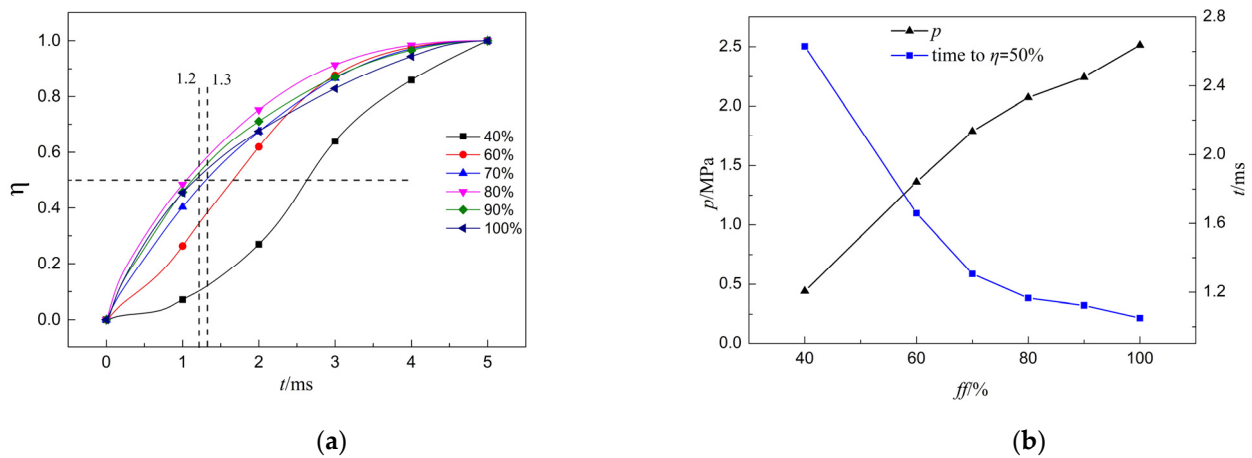


Figure 8. Radiation signal intensity of detonation and deflagration.

The ratio  $\eta$  of different fill fractions are calculated by the Equations (2) and (3). Figure 9a shows the ratio  $\eta$  at different times in the 350–1100 nm band of different fill fractions, where the detonation happens for fill fractions larger than 70% according to the laser absorption spectroscopy method. The plot shows that for fill fractions larger than 70%, the radiant energy increases rapidly when the wave arrives at time 0 ms, i.e., the ratio

$\eta$  increases rapidly. For fill fractions smaller than 70%, the radiant energy increases slowly when the wave arrives at time 0 ms, i.e., the ratio  $\eta$  increases slowly.



**Figure 9.** (a) The ratio  $\eta$  at different times in the 350–1100 nm band of different fill fractions, (b) Variation of pressure and the time to satisfy  $E_t = 50\%E_0$  (i.e.,  $\eta = 50\%$ ) of different fill fractions.

Figure 9b shows the variation of pressure and the time to satisfy  $E_t = 50\%E_0$  (i.e.,  $\eta = 50\%$ ) of different fill fractions. The plot shows that the pressure increases with the increase of fill fractions, while the time to satisfy  $\eta = 50\%$  decreases significantly. As mentioned above, the combustion mode is deflagration for fill fractions smaller than 70% according to the traditional method, and the corresponding time of  $\eta = 50\%$  is mainly larger than 1.3 ms. The combustion mode is detonation for fill fractions larger than 70% according to the traditional method, and the corresponding time of  $\eta = 50\%$  is mainly smaller than 1.2 ms. Therefore, the time interval of 1.2–1.3 ms can be used as the critical condition to identify the combustion mode, i.e., when the time of  $\eta = 50\%$  is smaller than 1.2 ms, the combustion mode is identified as detonation; on the contrary, when the time of  $\eta = 50\%$  is larger than 1.3 ms, the combustion mode is identified as deflagration. This method is named as the spectral radiation method.

Compared with the traditional pressure sensor test method, the spectral radiation method has obvious advantages in identifying the combustion mode: (1) By analyzing the visible radiation signal in the detonation process, the online monitoring of the performance of the detonation engine can be realized by obtaining the working state as well as the fill fraction of the detonation engine at the same time, while the traditional method can only realize the simultaneous measurements by using many more sensors. (2) The spectral radiation test is non-contact, which can avoid the problems of inconvenient installation of conventional contact test methods and sensibility to the environment temperature.

#### 4.3. Identify the Complete or Incomplete Combustion

In order to realize the process of deflagration to detonation quickly, obstacle configurations, such as orifice plate obstacle configuration and shchelkin spiral configuration, are mostly used in the detonation tube. In this paper, the detonation tubes used in the experiment adapted the configurations of seven orifice plate obstacles of 0.43 blockage ratio. The experiment shows that the gasoline droplets accumulated in the orifice plate obstacle configuration after the gasoline atomized by the ultrafine atomizing nozzle, which can result in excessive fuel in orifice plate obstacle configuration. The measurement results of CH and  $C_2$  radicals under different equivalence ratios show that  $C_2$  radicals appear more easily when the fuel is excessive [28].

In this section, the spectral signals of flames are measured by the high-resolution spectrometer, and the distribution of the main radicals (such as OH, CH and  $C_2$ ) are obtained. By analyzing the spectral signals of flames and distribution of radicals, the combustion state of the engine can be identified, and the chemical reaction mechanism of

gasoline can be verified experimentally. The transient radiation spectrum of detonation waves and detonation products at different times in the 200–1100 nm band measured by the spectrometer are shown in Figure 10.

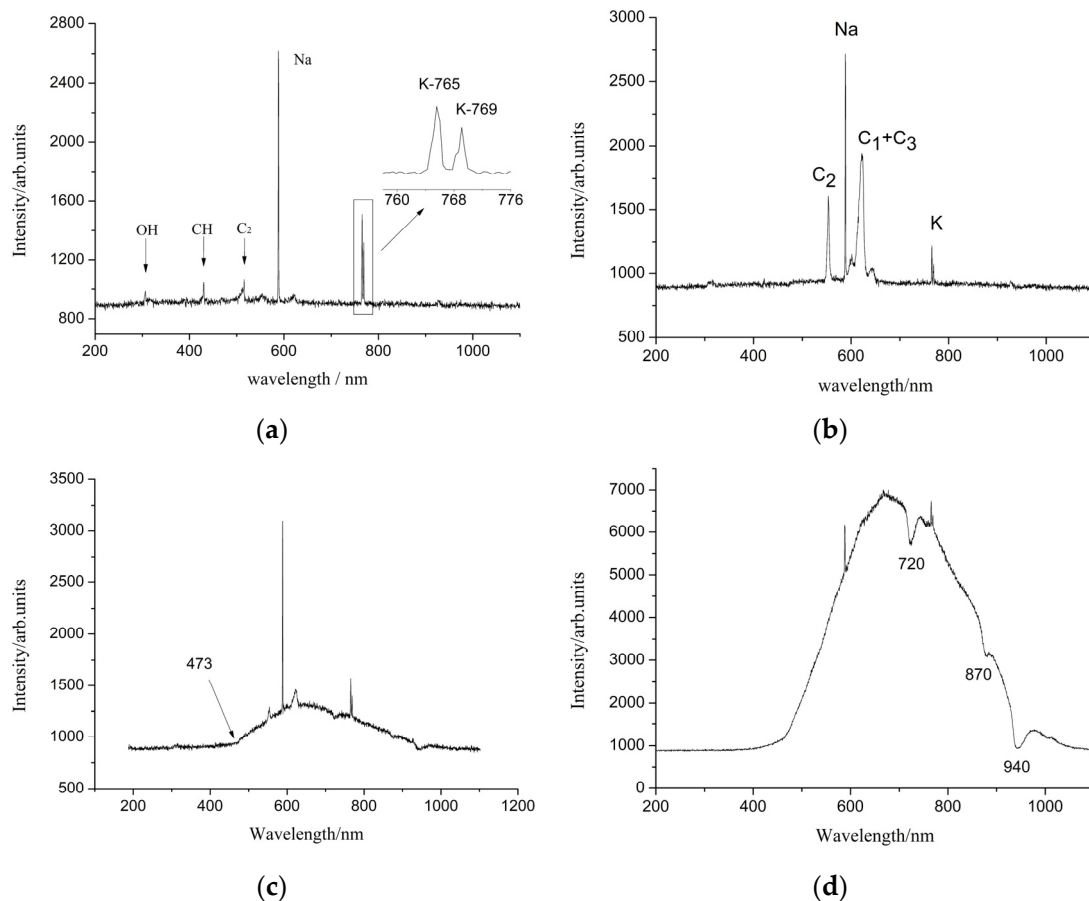


**Figure 10.** Radiation spectrum of detonation flame at different times: (a) 0 ms; (b) 10 ms; (c) 20 ms; (d) 50 ms.

As shown in Figure 10a, the characteristic spectra of  $C_2$ , CH, and OH radicals are obviously observed in the spectral signal, where the leading wavelength of  $C_2$ , CH, and OH spectrum bands are 516.5 nm, 431.4 nm, and 306.4 nm, respectively. The radiation intensity of  $C_2$  and CH radicals are significantly stronger than that of the OH radical. As the intensity of the radical spectrum is directly proportional to the radical concentration, the radiation intensity proves that the amount of  $C_2$  and CH radicals are comparative and much more than the OH radical in the process of chemical reaction.

The main components of gasoline are  $C_5$ – $C_{12}$  hydrocarbons, where the main elementary chemical reaction of the gasoline and air under the condition of ordinary combustion are  $C_2H + O \rightarrow C_2 + OH$  and  $CH_2 + O \rightarrow CH + OH$ . The CH and  $C_2$  radicals, as well as a small amount of OH radical, are produced intermediately during the chemical reaction. By comparing with the ordinary combustion, the concentration of  $C_2$  radical in detonation is much more obvious and the concentration of OH radical decreases in detonation, which can present the obvious differences in the formation mechanism of  $C_2$ , CH, and OH radicals in ordinary combustion and detonation [29]. The chemical reaction of  $C_2$  radical is known to increase the wave propagation velocity. Therefore, the velocity of detonation wave can be experimentally verified faster than that of the ordinary combustion wave.

The plots shown in Figure 10 show that in the 588 nm and 720 nm spectra, there are abnormally obvious atomic radiation signals. By comparing the characteristic spectral lines of NIST atomic spectrum database, the obvious atomic radiation signals are found to be consistent with the radiation signals of Na (588 nm) and K (765 nm, 769 nm), whose

spectral lines are 588 nm for Na and 765 nm or 769 nm for K. During the experiments, Na and K may come from impurity metals in gasoline or tube wall.

The plot shown in Figure 10b shows that the detonation flame is extinguished at 10 ms, and the radiation spectra of CH and OH radicals disappear with the ending of the chemical reaction. In addition to the obvious atomic radiation signals in the 588 nm and 720 nm spectra, there also exist obvious characteristic peaks in the 620 nm and 550 nm bands. Studies [28] have shown that the oxidant in the chemical reaction in the tube are obviously insufficient due to the turbulence effect of the obstacle configuration. The insufficient combustion caused by insufficient oxidant can result in large numbers of carbon black particles, C<sub>1</sub> radicals, C<sub>2</sub> radicals, and C<sub>3</sub> radicals. In the experiments with obstacle configuration, the characteristic peaks in the 620 nm and 550 nm bands, as shown in Figure 9b, can be recognized as the spectral lines of C<sub>2</sub> radical and the spectral lines of C<sub>1</sub>, as well as C<sub>3</sub>, radicals according to NIST database. Therefore, the existence of C<sub>1</sub> and C<sub>3</sub> radical radiation spectra can reflect whether the fuel is excessive and can be used as a monitoring object to improve the uniformity of fuel and oxidant in the detonation tube.

The plots shown in Figure 10d show that during 20 ms–50 ms, the residual high-temperature detonation products in the detonation tube are gradually exhausted, and the C radical signal gradually disappears. Continuous radiation spectral signals caused by high temperature solid carbon particles can be found in the 473 nm–1000 nm spectral band. Obvious absorption spectral signals of H<sub>2</sub>O during the detonation according to the HITRAN database can be found in 720 nm, 870 nm, and 940 nm spectral bands.

## 5. Conclusions

In this paper, the radiation spectrum and pressure of valveless multi-cycle gas–liquid two-phase PDE are studied experimentally. The radiation signal characteristics in 350–1100 nm, 800–1800 nm, and 1.2–2.6 μm bands, as well as the spectral signal characteristics of detonation in 200–1100 nm bands, are mainly analyzed. The main conclusions are as follows:

- (1) The radiation signals of filling process, ignition process, detonation waves exiting process, and detonation products exhausting process in a single working process of PDE are obtained experimentally. The analysis shows that each process has unique radiation signal characteristics. Based on the unique characteristics of radiation signals, a determination method of PDE fill fraction is proposed, i.e., the time spent in the detonation products exhausting process can be obtained according to the characteristics of radiation signals in each process, and then the filling condition of fuel in detonation tube can be calculated.
- (2) In this experimental study, the detonation and deflagration are found through pressure measurement. The radiation signals of detonation and deflagration are significantly different, and the radiation signal generated by detonation wave is much larger than that of the deflagration wave. It is found that when the detonation wave arrives, the radiation signal rises rapidly, and the radiation intensity is concentrated in the initial rising stage, while the radiation signal rises slowly, and the radiation intensity is relatively small for the deflagration wave arriving. These characteristics of radiation signals of detonation and deflagration can be used to identify the combustion state of PDE.
- (3) The spectral distributions of important intermediates during detonation, such as OH, CH, and C<sub>2</sub> radicals, are obtained from the radiation spectra of gasoline detonation, which are measured by the spectrometer. The results show that the concentration of C<sub>2</sub> and CH radicals are significantly higher than that of OH radicals. By analyzing the radiation spectra signals of detonations under excessive fuel and uneven fuel–oxidant distributions, large numbers of C<sub>1</sub> and C<sub>3</sub> radicals are found for incomplete combustion. Therefore, the existence of C<sub>1</sub> and C<sub>3</sub> radical radiation spectra can reflect the mixing uniformity or equivalence ratio of fuel and oxidant and can be used to identify the complete or incomplete combustion of fuel online.

In conclusion, the optical diagnostic method based on radiation in visible and near-infrared region would serve as a helpful approach to realize accurate control of pulsed detonation engine in flight tests, where observation windows or complex optical systems are no longer allowed. Additional radiation information about the detonation status would help operational staff to estimate the engine states online. Moreover, the radiation method mentioned in this paper would also be a powerful tool for optical diagnostic in other engines with the pulse property, such as a pulsed jet engine.

**Author Contributions:** Conceptualization, X.H. and N.L.; methodology, N.L.; formal analysis, X.H.; investigation, X.H., N.L. and Y.K.; data curation, X.H. and Y.K.; writing—original draft preparation, X.H.; writing—review and editing, X.H.; supervision, X.H.; project administration, N.L.; funding acquisition, N.L. All authors have read and agreed to the published version of the manuscript.

**Funding:** This research was funded by the China Scholarship Council (contract 201906845059), the Young Scientists Fund of the Natural Science Foundation of Jiangsu Province (No. BK20190439), the Fundamental Research Funds of National Key Laboratory of Transient Physics (No. 6142604200202).

**Institutional Review Board Statement:** Not applicable.

**Informed Consent Statement:** Not applicable.

**Data Availability Statement:** The data presented in this study are available on request from the corresponding author.

**Conflicts of Interest:** The authors declare no conflict of interest.

## References

1. Lee, J.H.S. *The Detonation Phenomenon*, 1st ed.; Cambridge University Press: New York, NY, USA, 2008; pp. 1–10.
2. Rosato, D.A.; Thornton, M.; Sosa, J.; Bachman, C.; Ahmed, K.A. Stabilized detonation for hypersonic propulsion. *Proc. Natl. Acad. Sci. USA* **2021**, *118*, 1–10. [[CrossRef](#)]
3. Batista, A.; Ross, M.C.; Lietz, C.; Hargus, W.A. Descending modal transition dynamics in a large eddy simulation of a rotating detonation rocket engine. *Energies* **2021**, *14*, 3387. [[CrossRef](#)]
4. Li, J.M.; Teo, C.J.; Khoo, B.C.; Wang, J.P.; Wang, C. *Detonation Control for Propulsion: Pulse Detonation and Rotating Detonation Engines*, 1st ed.; Springer International Publishing: Cham, Switzerland, 2018; pp. 183–198.
5. Hanafi, A.M.; Mark, S. Pulse detonation assessment for alternative fuels. *Energies* **2017**, *10*, 369.
6. Matsuoka, K.; Taki, H.; Kawasaki, A.; Kasahara, J.; Watanabe, H.; Matsuo, A.; Endo, T. Semi-valveless pulse detonation cycle at a kilohertz-scale operating frequency. *Combust. Flame* **2019**, *205*, 434–440. [[CrossRef](#)]
7. Frolov, S.M.; Smetanyuk, V.A.; Gusev, P.A.; Koval, A.S.; Nabatnikov, S.A. How to utilize the kinetic energy of pulsed detonation products? *Appl. Therm. Eng.* **2019**, *147*, 728–734. [[CrossRef](#)]
8. Frolov, S.M.; Aksenov, V.S.; Ivanov, V.S.; Shamshin, I.O.; Nabatnikov, S.A. Catapult launching tests of an unmanned aerial vehicle with a ramjet pulsed-detonation engine. *Combust. Explo.* **2019**, *12*, 1–11.
9. Kim, J.M.; Han, H.S.; Choi, J.Y. The experimental study about the effect of operating conditions on multi-tube pulse detonation engine performance. *Int. J. Aeronaut. Space* **2018**, *19*, 89–99. [[CrossRef](#)]
10. Anand, V.; George, A.S.; Knight, E.; Gutmark, E. Investigation of pulse detonation combustors—Axial turbine system. *Aerosp. Sci. Technol.* **2019**, *93*, 105350. [[CrossRef](#)]
11. Anand, V.; Glaser, A.; Gutmark, E. Acoustic characterization of pulse detonation combustors. *AIAA J.* **2018**, *56*, 2806–2815. [[CrossRef](#)]
12. Haghdoost, M.R.; Edgington-Mitchell, D.; Paschereit, C.O.; Oberleithner, K. High-speed Schlieren and particle image velocimetry of the exhaust flow of a pulse detonation combustor. *AIAA J.* **2020**, *58*, 3527–3543. [[CrossRef](#)]
13. Bradley, D.; Lawes, M.; Liu, K. Turbulent flame speeds in ducts and the deflagration/detonation transition. *Combust. Flame* **2008**, *154*, 96–108. [[CrossRef](#)]
14. Liu, C.; Xu, L. Laser absorption spectroscopy for combustion diagnosis in reactive flows: A review. *Appl. Spectrosc. Rev.* **2019**, *54*, 1–44. [[CrossRef](#)]
15. Matsuoka, K.; Esumi, M.; Ikeguchi, K.B.; Kasahara, J.; Matsuo, A.; Funaki, I. Optical and thrust measurement of a pulse detonation combustor with a coaxial rotary valve. *Combust. Flame* **2012**, *159*, 1321–1338. [[CrossRef](#)]
16. Hanraths, N.; Bohon, M.D.; Paschereit, C.O.; Djordjevic, N. Unsteady effects on NOx measurements in pulse detonation combustion. *Flow Turbul. Combust.* **2021**, *7*, 1–29.
17. Nations, M.; Wang, S.; Goldenstein, C.S.; Sun, K.; Davidson, D.F.; Jeffries, J.B.; Hanson, R.K. Shock-tube measurements of excited oxygen atoms using cavity-enhanced absorption spectroscopy. *Appl. Opt.* **2015**, *54*, 8766–8775. [[CrossRef](#)]
18. Goldenstein, C.S.; Spearrin, R.M.; Jeffries, J.B.; Hanson, R.K. Infrared laser absorption sensors for multiple performance parameters in a detonation combustor. *P. Combust. Inst.* **2015**, *35*, 3739–3747. [[CrossRef](#)]

19. Goldenstein, C.S.; Schultz, I.A.; Spearrin, R.M.; Jeffries, J.B.; Hanson, R.K. Scanned-wavelength-modulation spectroscopy near 2.5  $\mu\text{m}$  for  $\text{H}_2\text{O}$  and temperature in a hydrocarbon-fueled scramjet combustor. *Appl. Phys. B* **2014**, *116*, 717–727. [[CrossRef](#)]
20. Li, F.; Yu, X.; Cai, W.; Ma, L. Uncertainty in velocity measurement based on diode-laser absorption in nonuniform flows. *Appl. Opt.* **2012**, *51*, 4788–4797. [[CrossRef](#)] [[PubMed](#)]
21. Hinckley, K.; Jeffries, J.; Hanson, R. A wavelength-multiplexed diode laser sensor for temperature measurements in detonation engines. In Proceedings of the 42nd AIAA Aerospace Sciences Meeting and Exhibit, Reno, NV, USA, 5–8 January 2004; pp. 2004–2713.
22. Ma, L.; Jeffries, J.; Hanson, R.; Hinckley, K.; Pinard, P.; Dean, A. Characterization of the fuel fill process in a multi-cycle pulse detonation engine using a diode-laser sensor. In Proceedings of the 41st AIAA/ASME/SAE/ASEE Joint Propulsion Conference & Exhibit, Tucson, AZ, USA, 10–13 July 2005; pp. 2005–3834.
23. Lv, X.J.; Li, N.; Weng, C.S. Research on diagnosis of gas-liquid detonation exhaust based on double optical path absorption spectroscopy technique. *Spectrosc. Spect. Anal.* **2014**, *34*, 582–586.
24. Hu, H.B.; Weng, C.S.; Lv, X.J.; Li, N. Analysis on impulse characteristics of pdre with exhaust measurements. *Int. J. Turbo Jet Eng.* **2014**, *31*, 97–103. [[CrossRef](#)]
25. Rankin, B.A.; Codoni, J.R.; Cho, K.Y.; Hoke, J.L.; Schauer, F.R. Investigation of the structure of detonation waves in a non-premixed hydrogen-air rotating detonation engine using mid-infrared imaging. *P. Combust. Inst.* **2019**, *37*, 3479–3486. [[CrossRef](#)]
26. White, L.W.; Feleo, A.; Gamba, M. Mid-infrared pulsed upconversion imaging in a rotating detonation combustor. *AIAA Scitech 2021 Forum* **2021**, 0419. [[CrossRef](#)]
27. Lv, X.J.; Li, N.; Weng, C.S. Research on filling process of fuel and oxidant during detonation based on absorption spectrum technology. In *International Symposium on Optoelectronic Technology and Application 2014: Laser and Optical Measurement Technology; and Fiber Optic Sensors*; International Society for Optics and Photonics: Bellingham, WA, USA, 2014; Volume 9297, p. 92970V.
28. Köhler, M.; Brockhinke, A.; Braun-Unkhoff, M.; Kohse-Höinghaus, K. Quantitative laser diagnostic and modeling study of  $\text{C}_2$  and CH chemistry in combustion. *J. Phys. Chem. A* **2010**, *114*, 4719–4734. [[CrossRef](#)] [[PubMed](#)]
29. Li, Y.L.; He, J.N.; Zhang, C.H.; Li, P.; Li, X.Y. Research on the time-histories of exited radicals during the combustion of methylcyclohexane by emission spectroscopy. *Spectrosc. Spect. Anal.* **2016**, *36*, 11–14.